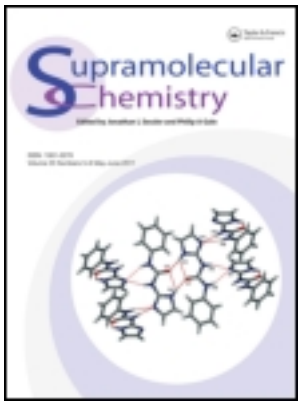

Supramolecular Chemistry
Publication details, including instructions for authors and subscription information:
http://www.tandfonline.com/loi/gsch20

Self-assembly of tert-butyl silanetriol in solution and aggregation with tetrahydrofuran

Stefan Spirk [a], Stefan Salentinig [a], Klaus Zangger [a], Ferdinand Belaj [a] & Rudolf Pietschnig [a] [b]

[a] Institut für Chemie, Karl-Franzens-Universität Graz, Graz, Austria
[b] Institut für Chemie, Universität Kassel, Heinrich-Plett-Str. 40, 34132, Kassel, Germany

Available online: 28 Nov 2011

To cite this article: Stefan Spirk, Stefan Salentinig, Klaus Zangger, Ferdinand Belaj & Rudolf Pietschnig (2011): Self-assembly of tert-butyl silanetriol in solution and aggregation with tetrahydrofuran, Supramolecular Chemistry, 23:12, 801-805

To link to this article: http://dx.doi.org/10.1080/10610278.2011.622380

Supramolecular Chemistry
Vol. 23, No. 12, December 2011, 801–805

Taylor & Francis
Taylor & Francis Group

Self-assembly of *tert*-butyl silanetriol in solution and aggregation with tetrahydrofuran

Stefan Spirk[a], Stefan Salentinig[a], Klaus Zangger[a], Ferdinand Belaj[a] and Rudolf Pietschnig[a,b]*

[a]*Institut für Chemie, Karl-Franzens-Universität Graz, Graz, Austria;* [b]*Institut für Chemie, Universität Kassel, Heinrich-Plett-Str. 40, 34132 Kassel, Germany*

(*Received 15 April 2011; final version received 26 August 2011*)

tert-Butyl silanetriol behaves like a surfactant and self-assembles in aqueous and tetrahydrofuran (THF) solutions. Micelle formation was studied with pulsed field gradient stimulated spin echo (PFG-SSE) NMR, while multilayer lamellar vesicles can be concluded from small/wide angle X-ray scattering measurements in concentrated solutions at elevated temperature. The significant interaction between *tert*-butyl silanetriol and THF is further highlighted by a crystal structure featuring a 3:1 adduct of silanetriol and THF.

Keywords: silanol; hydrogen bond; micelle

Introduction

Silanols are the silicon analogues of alcohols containing one or more Si—OH groups. Transient silanols are important in a variety of industrial applications such as the manufacture of silicones, sol–gel processes and as silane-coupling agents for use in the functionalisation of surfaces (*1*). Unlike their carbon counterparts, several hydroxyl functions can be attached to the same silicon atom and the tendency to participate in hydrogen bonding increases with the number of silanol functions in the molecule. In the case of silanetriols, $R—Si(OH)_3$, the maximum number of silanol functions is available for a neutral organosilanol. In recent years, stable silanetriols have become attractive synthetic goals, and their rich structural chemistry has been explored extensively in the solid state (*2,3*). Some control over the structural organisation of silanetriols has been achieved by the variation of the pertinent organic substituent (*2–5*). It has been demonstrated that with the same substituent different structural motifs can be obtained depending on the crystallisation conditions (*6*).

The *tert*-butyl-substituted silanetriol is known to be robust and easy to synthesise (*5,7*). Recently, *tert*-butyl silanetriol **1** has been used to prepare polyhedral oligomeric silsesquioxane-type cages and surface coatings under mild conditions (*8,9*). Here, we report our results on the association behaviour of **1** in solution. The formation of aggregates of *tert*-butyl silanetriol has been explored using pulsed field gradient stimulated spin echo (PFG-SSE) NMR experiments and small/wide angle X-ray scattering (SAXS/WAXS) methods. To our knowledge, this is the first time that the self-association of silanetriols in solution has been explored.

Results and discussion

One of the most important aspects of silanol chemistry is the relatively high polarity of the Si—OH group (*2*). Accordingly, silanols in general and silanetriols in particular should be well suited as surfactants. Considering the possibility of interaction of silanetriol molecules in solution, association might occur via hydrogen bonding or via electrostatic or dispersive interactions (Scheme 1).

The critical micelle concentration (CMC) is the concentration which is needed for the self-assembly of individual molecules to aggregate via the above-mentioned attractive forces. An elegant way to explore such aggregation in solution is PFG-SSE NMR (*10*). By measuring the diffusion coefficients of the compound of interest as a function of its concentration, the size of the aggregates formed can be determined according to the Stokes–Einstein equation (Equation (1) with D, diffusion coefficient; k_b, Boltzmann's constant; T, absolute temperature; η, dynamic viscosity; R_H, hydrodynamic radius of a spherical particle):

$$R_H = \frac{k_b T}{6\pi\eta D}. \quad (1)$$

In the case of silanetriol **1**, the diffusion coefficients of the methyl protons were determined using ^{1}H NMR spectroscopy (Figure 1).

For solutions containing less than 1.0 wt% of **1**, calculated hydrodynamic radii are 4–5 Å. These hydrodynamic radii fit very well with the size of only a few (i.e. 1–3) individual silanetriol molecules. It is thus obvious that this concentration range is below the CMC. For solutions of **1** at higher concentrations the hydrodynamic

*Corresponding author. Email: pietschnig@uni-kassel.de

ISSN 1061-0278 print/ISSN 1029-0478 online

http://dx.doi.org/10.1080/10610278.2011.622380
http://www.tandfonline.com

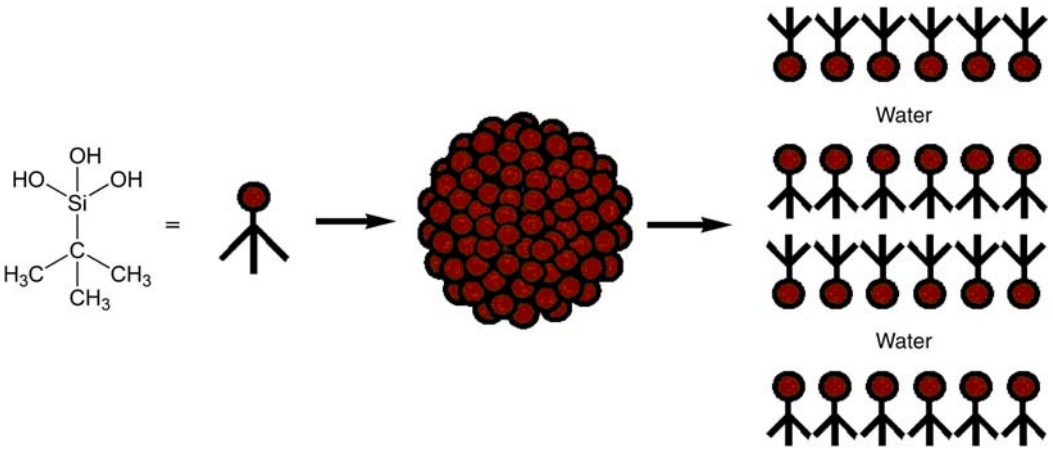

Scheme 1. Illustration of the aggregation of **1** in aqueous solution.

radii increase to *ca.* 40 Å, which corresponds to an assembly of *ca.* 1400 molecules per aggregate assuming a packing density similar to the one observed for the unsolvated silanetriol in the solid state based on single-crystal X-ray diffraction (*5*). In comparison, partially solvated structures as discussed later in the article (Figures 3 and 4) would correspond to approximately 1200 molecules per aggregate based on the packing density of the corresponding single-crystal X-ray diffraction data.

For an insight into the internal structure of the aggregates other techniques have to be applied, such as SAXS and WAXS, which are widely used for this purpose (*11*). In an initial attempt, we investigated solutions of **1** with SAXS at the same concentrations used in the NMR experiments. Owing to the insufficient scattering behaviour of our samples in this concentration range, we had to turn to more concentrated solutions of **1** in order to apply this technique (the limited solubility of **1** in water can be overcome at elevated temperatures). Thus, concentrated solutions of 50 wt% of **1** can be easily obtained as clear low-viscosity solutions at different temperatures (50, 70 and 90°C). The SAXS/WAXS curves of **1** at these temperatures are, however, identical and therefore we only refer to the 90°C case in the following because the viscosity of the solution is lowest for this temperature.

On the basis of these experiments, it can be concluded that multilamellar vesicles were formed showing bilayer or multilayer structural motifs, at least in the high concentration range. The occurrence of equidistant peaks (e.g. 6.1, 12.2 and 18.3 nm^{-1}) is indicative of multilayer structural motifs and, moreover, affords information about the interlamellar distance *d,* which can be obtained by combining Bragg's law with the definition of the scattering vector q derived from the relationship $d = 2\pi/q$.

It is likely that similar to the crystal structure of **1** the hydrophobic *tert*-butyl groups are arranged so as to

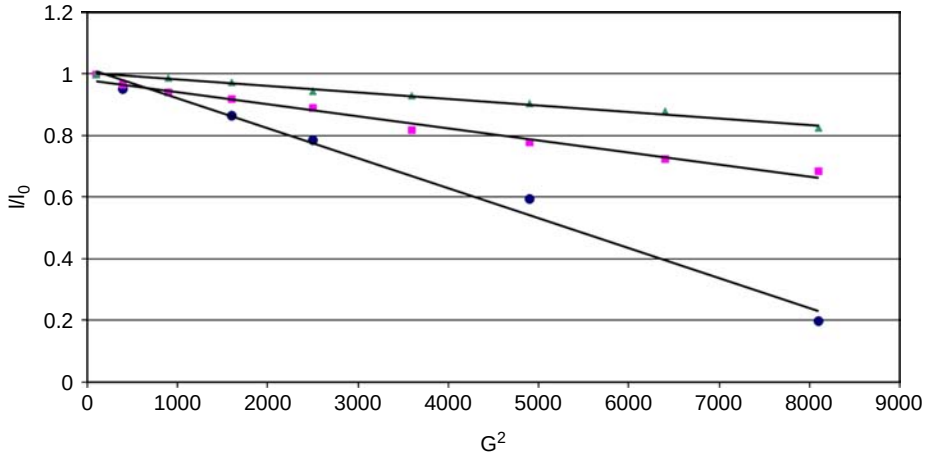

Figure 1. Plot of the intensity decay versus the square of the gradient strength for aqueous solutions of **1** at different concentrations (circle: 0.06 wt%, square: 0.56 wt%, triangle: 1.7 wt%, $T = 298$ K). The self-diffusion coefficients were obtained from the slopes of the straight lines as described in the Experimental section.

minimise exposure to polar units and solvent (water) while the silanol units do just the opposite. This is indicated by the shape of the peaks which shows the so-called fronting and therefore suggests an orientation of the sample molecules towards the glass surface of the sample container (*12*). The interlamellar distance of about 1.0 nm compares well with the Si1—O—H···Si1′—O—H distance of 0.98 nm in the crystal structure of **1** (*5,7*). Similar results have been obtained for concentrated (40 wt%) solutions of **1** in tetrahydrofuran (THF; Figure 2). The smaller peaks may be attributed to other possibly disordered liquid crystalline phases but cannot be assigned unambiguously.

Quantum chemical calculations suggest that the interaction of silanols is in fact stronger with ethers than with water (*13*). Consistent with this, we have been able to obtain crystals from concentrated solutions of **1** in THF, the composition of which can be described as adducts of silanetriol **1** and THF in a 3:1 ratio. The crystals were suitable for single-crystal X-ray diffraction, and a plot of the asymmetric unit is depicted in Figure 3.

The crystal structure analysis confirmed the compound as $C_4H_9Si(OH)_3$* 1/3 THF. The asymmetric unit (Figure 3) consists of a semicircle of three $C_4H_9Si(OH)_3$ molecules held together by two hydrogen bonds between two molecules and a disordered THF molecule hydrogen bonded to a terminal OH group of this aggregate. All three crystallographically different $C_4H_9Si(OH)_3$ molecules have further double hydrogen bonds arranged around inversion centres with their symmetry-related neighbour molecules. By these hydrogen bonds, a 2D aggregate parallel to the (110) plane is formed (Figure 4): six $C_4H_9Si(OH)_3$ molecules build circles with two THF molecules in the centre, and these circle-shaped aggregates of slightly <20 Å diameter are connected in a pseudo-hexagonal manner to six further aggregates by inversion

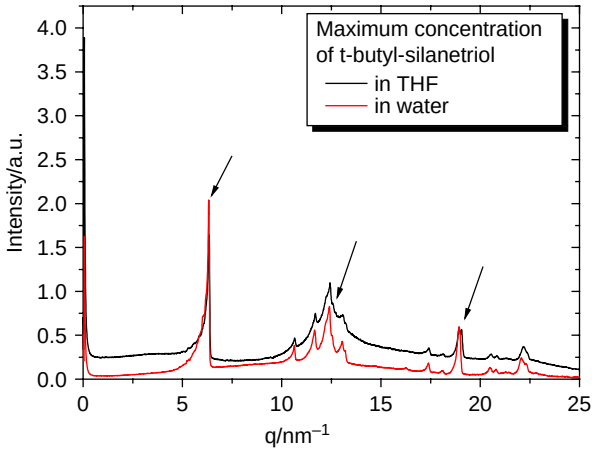

Figure 2. SAXS/WAXS patterns for highly concentrated aqueous solutions of **1** at 50 wt% in water (90°C) and 40 wt% in THF (40°C). The arrows mark the equidistant peaks for the lamellar phase.

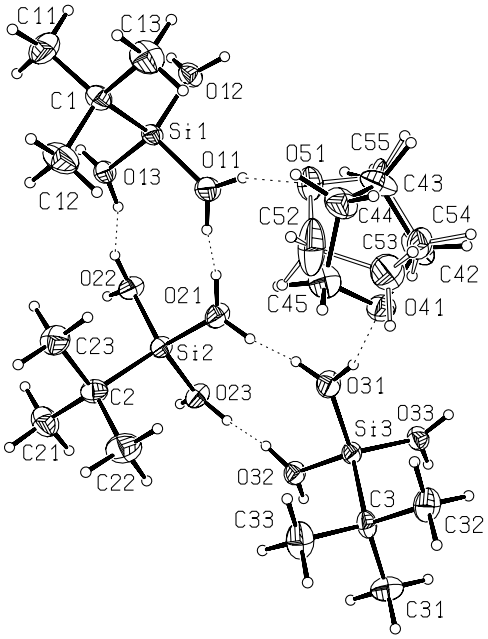

Figure 3. ORTEP plot of the asymmetric unit of **1**· *1/3 THF* showing the atomic numbering scheme. The THF molecule having the smaller site occupation factor of 0.431(7) is drawn with open bonds, the hydrogen bonds are indicated by dashed lines. The probability ellipsoids are drawn at the 50% probability level.

centres lying on the face centres and edge centres at $c = 0.5$. According to their structural parameters, all the 18 hydrogen bonds (Table 1) can be classified as strong [O···O $\leq$ 2.718(3) Å, O—H···O $\geq$ 155(4)°] and have disordered H atoms (*14*). The $C_4H_9Si(OH)_3$ molecules show staggered conformations [$|\tau_{O\text{-}Si\text{-}C\text{-}C}| \geq 176.0(2)°$],

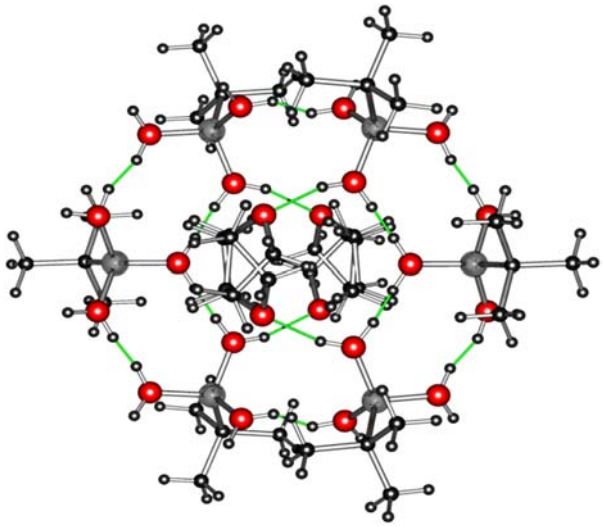

Figure 4. POV-Ray plot of two asymmetric units of **1**· *1/3* THF related by a centre of inversion. The atoms are drawn with arbitrary radii and the hydrogen bonds are plotted with dark lines.

Table 1. Hydrogen bonds for **1**· *1/3 THF* [Å, °].

D-H···A	d(D–H)	d(H···A)	d(D···A)	<(DHA)
O(11)—H(111)···O(51)	0.84	1.749(18)	2.536(6)	155(4)
O(11)—H(112)···O(21)	0.84	1.856(6)	2.691(3)	172(4)
O(12)—H(121)···O(33)[a]	0.84	1.870(2)	2.666(3)	158(5)
O(12)—H(122)···O(13)[b]	0.84	1.874(14)	2.695(3)	166(6)
O(13)—H(131)···O(12)[b]	0.84	1.862(11)	2.695(3)	171(7)
O(13)—H(132)···O(22)	0.84	1.888(11)	2.718(3)	169(6)
O(21)—H(212)···O(31)	0.84	1.838(8)	2.675(3)	173(7)
O(21)—H(211)···O(11)	0.84	1.858(9)	2.691(3)	171(5)
O(22)—H(221)···O(23)[c]	0.84	1.867(13)	2.697(3)	169(7)
O(22)—H(222)···O(13)	0.84	1.899(17)	2.718(3)	165(6)
O(23)—H(231)···O(32)	0.84	1.865(3)	2.705(3)	177(3)
O(23)—H(232)···O(22)[c]	0.84	1.861(5)	2.697(3)	174(4)
O(31)—H(312)···O(41)	0.84	1.745(7)	2.558(5)	162(2)
O(31)—H(311)···O(21)	0.84	1.849(15)	2.675(3)	167(7)
O(32)—H(321)···O(33)[d]	0.84	1.864(6)	2.702(3)	175(7)
O(32)—H(322)···O(23)	0.84	1.869(4)	2.705(3)	173(3)
O(33)—H(331)···O(12)[a]	0.84	1.846(5)	2.666(3)	165(2)
O(33)—H(332)···O(32)[d]	0.84	1.866(9)	2.702(3)	173(7)

Notes: Symmetry transformations used to generate equivalent atoms: [a]1–x, 1–y, 1–z; [b]1–x, –y, 1–z; [c]2–x, –y, 1–z; [d]2–x, 1–y, 1–z.

the Si—O bond length of the atoms On1 ($n = 1–3$) is slightly smaller [1.617(2)–1.621(2) Å] than those of the other O atoms [1.632(2)–1.638(2) Å]. It should be mentioned that the incorporation of solvent into silanetriol structures is not unprecedented and examples including water (*6,15,16*) and alcohol (*16*) have been previously reported.

Conclusion

In conclusion, we have shown that *tert*-butyl silanetriol behaves like a polar surfactant molecule and self-assembles in aqueous solution. In dilute solution, we found that micelles form above 1 wt% (NMR) while at high concentrations (50 wt%) multilayer lamellar vesicles can be concluded from SAXS/WAXS measurements. Similar results were obtained in concentrated THF solutions indicating that this phenomenon is not limited to water as a solvent. In addition, the significant interaction between *tert*-butyl silanetriol and THF is further highlighted by a crystal structure featuring a 3:1 adduct of silanetriol and THF. Given the high tendency of silanols to form hydrogen bonds and the recent interest in liquid hydrogen-bonded networks as reaction media for catalytic transformations (*17*), silanols might be environmentally benign and sustainable alternatives to the fluoroalcohols currently employed for this purpose.

Experimental details

Materials and sample preparation

Silanetriol **1** was prepared according to published procedures (*5,7*) and recrystallised twice from ether. NMR measurements were obtained on a Bruker Avance DRX 500 MHz NMR spectrometer. To confirm the stability of **1** in D_2O, variable temperature (VT)-NMR experiments were performed starting at 298 K with increments of 10 K and a concentration of 1 wt% of **1**. After each increase, the temperature was maintained for 10 min to ensure the thermal equilibration of the sample. After reaching the maximum temperature (373 K) the probe was cooled to 298 K. This procedure was repeated twice. For highly concentrated solutions, a starting temperature of 373 K was used. As mentioned above, no sign of decomposition was observed.

Self-diffusion coefficients were obtained by measuring a series of nine pulsed gradient spin echo (PGSE) spectra by varying the gradient strengths. The signal intensity was least squares fitted to the equation

$$\ln(I) = a - bDG^2, \quad (2)$$

with I, signal intensity; G, the gradient strength and D, self-diffusion coefficient. All other parameters were combined to the instrument-dependent constants a and b, which were obtained by a calibration on a system where the self-diffusion coefficient was known. This calibration was carried out with a sample containing 90% H_2O and 10% D_2O and the temperature-corrected H_2O diffusion coefficient of 2.49×10^{-9} m^2/s (*18,19*).

Samples containing up to 5 wt% of *tert*-butylsilanetriol were prepared by adding silanetriol **1** and a defined amount of twice-distilled water on the balance into a 4-ml vial. For highly concentrated solutions of the amphiphile, samples were prepared by mixing the solid component into water at elevated temperature, depending on the solubilisation limit of the component in water and THF. We therefore used 4-ml vials that could be sealed with a cap to prevent evaporation of the solvent during the heating and mixing procedure which was performed by vortexing the sample. After some seconds, the hot solution became clear. For our SAXS measurements and for the investigation of the sample by NMR, we focused on samples at 90°C with water as a solvent and at 40°C for THF samples.

Small/wide angle X-ray scattering

The multilamellar phases of the particles were investigated by a SAXS/WAXS technique. Our equipment comprises a SAXSess camera (Anton-Paar, Graz, Austria), connected to an X-ray generator (Philips, PW 1730/10) operating at 40 kV and 50 mA with a sealed-tube Cu anode. A Göbel mirror was used to convert the divergent polychromatic X-ray beam into a focused line-shaped beam of Cu K_α radiation ($\lambda = 0.154$ nm). The 2D scattering pattern was recorded by an imaging-plate detector (Fuji BAS1800 from Raytest, Straubenhardt,

Germany) or by a PI-SCX-fused fibre optic taper CCD camera from Princeton Instruments (division of Roper Scientific, Inc., Trenton, NJ, USA), and integrated into the 1D scattering function $I(q)$. The SAXSess system also facilitates WAXS experiments. Imaging plates were used to record WAXS patterns up to $q = 25\,\mathrm{nm}^{-1}$. The CCD detector that was used features a 2084×2084 array with $24 \times 24\,\mu\mathrm{m}$ pixel size (chip size: $50 \times 50\,\mathrm{mm}$) at a sample-to-detector distance of 311 mm. The CCD is operated at -30°C with 10°C water-assisted cooling to reduce the thermally generated charge. Cosmic ray correction and background subtraction were made on the 2D image before further data processing. The images are then integrated into the 1D scattering function $I(q)$, where q is the scattering vector defined by $q = (4\pi/\lambda)\sin(\theta/2)$, where λ is the wavelength and θ is the scattering angle.

The temperature of the capillary and the metallic sample holder was controlled by a Peltier element. Samples were equilibrated at the desired temperature for 30 min before each measurement. Using the set-up with a CCD camera, dispersions were exposed to X-rays for 10 min, three times for averaging, whereas with the image plate device they were measured for 45 min. The lamellar phase was determined by the relative positions of the scattering peaks displayed in the scattering curves, which correspond to the reflections on planes defined by their (*hkl*) Miller indices.

Single-crystal X-ray diffraction

X-ray diffraction data of **1**· *1/3 THF*: All measurements were obtained using graphite-monochromated Mo K_α radiation at 95 K: $3C_4H_9Si(OH)_3 \cdot C_4H_8O$, M_r 480.78, triclinic, space group P-1, $a = 11.731(5)$ Å, $b = 11.794(5)$ Å, $c = 12.197(5)$ Å, $\alpha = 85.36(3)°$, $\beta = 63.46(3)°$, $\gamma = 63.33(3)°$, $V = 1333.9(11)$ Å^3, $Z = 2$, $d_{calc} = 1.197\,\mathrm{g\,cm}^{-3}$, $\mu = 0.220\,\mathrm{mm}^{-1}$. A total of 6211 reflections were collected ($\Theta_{max} = 26.0°$) of which 5239 were unique ($R_{int} = 0.0470$), with 3599 having $I > 2\sigma(I)$. The structure was solved by direct methods (SHELXS-97) and refined by full-matrix least-squares techniques against F^2 (SHELXL-97). The non-hydrogen atoms were refined with anisotropic displacement parameters. The THF molecules are disordered over two orientations and were refined with site occupation factors of 0.569(7) and 0.431(7), respectively. The equivalent bonds in these solvent molecules are restrained to have the same lengths. The H atoms of the methyl groups were refined with common isotropic displacement parameters for the H atoms of the same group and idealised geometry with tetrahedral angles, enabling rotation around the X—C bond and C—H distances of 0.98 Å. The H atoms of the CH_2 groups were refined with common isotropic displacement parameters for the H atoms of the same group and idealised geometry with approximately tetrahedral angles and C—H distances of 0.99 Å. The H atoms of the OH groups are disordered over two sites. They were refined with site occupation factors of 0.5 and with common isotropic displacement parameters for the H atoms bonded to the same O atom. The bond length was fixed to be 0.84 Å. For 392 parameters, final R indices of $R1 = 0.0580$ and $wR^2 = 0.1387$ (GOF = 1.016) were obtained. The largest peak in a difference Fourier map was $0.328\,\mathrm{eÅ}^{-3}$. The CCDC deposition number is 821876.

Acknowledgements

The authors would like to thank the Austrian Science Fund (FWF) for financial support. The authors would also like to thank Otto Glatter for stimulating discussions.

References

(1) Brook, A.G. In *The Chemistry of Organic Silicon Compounds*; Rappoport, Z., Apeloig, Y., Eds.; Wiley: New York, 1998; Vol. 2.
(2) Lickiss, P.D. *Adv. Inorg. Chem.* **1995**, *42*, 147–262.
(3) Lickiss, P.D. In *Chemistry of Organic Silicon Compounds*; Rappoport, Z., Apeloig, Y., Eds.; Wiley: Chichester, UK, 2001; Vol. 3, pp 695–744.
(4) Pietschnig, R.; Belaj, F.; Tirrée, J.J. *Organometallics* **2004**, *23*, 4897–4901.
(5) Pietschnig, R.; Belaj, F. *Inorg. Chim. Acta* **2005**, *358*, 444–448.
(6) Spirk, S.; Belaj, F.; Baumgartner, J.; Pietschnig, R. *Z. Anorg. Allg. Chem.* **2009**, *635*, 1048–1053.
(7) Winkhofer, N.; Roesky, H.W.; Noltemeyer, M.; Robinson, W.T. *Angew. Chem.* **1992**, *104*, 670–671.
(8) Spirk, S.; Ehmann, H.; Reischl, M.; Kargl, R.; Hurkes, N.; Wu, M.; Novak, J.; Resel, R.; Pietschnig, R.; Ribitsch, V. *Appl. Mat. Interf.* **2010**, *2*, 2956–2962.
(9) Spirk, S.; Nieger, M.; Belaj, F.; Pietschnig, R. *Dalton Trans.* **2009**, 163–167.
(10) Tanner, J.E. *J. Chem. Phys.* **1970**, *52*, 2523–2526.
(11) Glatter, O.; Kratky, O. *Small Angle X-Ray Scattering*; Academic Press: London, 1982.
(12) Yaghmur, A.; de Campo, L.; Salentinig, S.; Sagalowicz, L.; Leser, M.E.; Glatter, O. *Langmuir* **2006**, *22*, 517–521.
(13) Beckmann, J.; Grabowsky, S. *J. Phys. Chem.* **2007**, *111*, 2011–2019.
(14) Steiner, T. *Angew. Chem. Int. Ed.* **2002**, *41*, 48–76.
(15) Jutzi, P.; Strassburger, G.; Schneider, M.; Stammler, H.-G.; Neumann, B. *Organometallics* **1996**, *15*, 2842–2844.
(16) Schneider, M.; Neumann, B.; Stammler, H.G.; Jutzi, P. *Monatsh. Chem.* **1999**, *130*, 33–44.
(17) Berkessel, A. *Nachr. Chem.* **2008**, *56*, 126–130.
(18) Longsworth, L. *J. Phys. Chem.* **1960**, *64*, 1914–1917.
(19) Mills, R. *J. Phys. Chem.* **1972**, *77*, 685–688.